Journal of King Saud University – Engineering Sciences 31 (2019) 78–85

Contents lists available at ScienceDirect

Journal of King Saud University – Engineering Sciences

journal homepage: www.sciencedirect.com

Original article

Synthesis and characterisation of iron millscale particles reinforced ceramic matrix composite

O.I. Sekunowo, S.I. Durowaye *, G.I. Lawal

Department of Metallurgical and Materials Engineering, University of Lagos, Akoka, Lagos, Nigeria

ARTICLE INFO

Article history:
Received 9 June 2016
Accepted 21 March 2017
Available online 22 March 2017

Keywords:
Iron millscale
Ceramic matrix composite
Brake pad
Characterisations

ABSTRACT

A promising sintered particulate ceramic matrix composite suitable for automobiles and aircrafts brake pad application was developed by powder metallurgy method in an attempt to enhance the performance and service life of the brake pad. The detailed methodology involves using formulation of 30 wt% silica, 40 wt% magnesia, and 30 wt% bentonite as matrices. The blended matrix was reinforced with iron millscale particles which varied from 3 to 18 wt% at particles size distribution (106–250) μm. The developed composites were subjected to physical, mechanical, thermal, wear, and microstructural characterisations using Scanning Electron Microscopy with Energy Dispersive Spectroscopy (SEM/EDS). Microstructure of the composite shows a uniform distribution of millscale particles in the ceramic matrix with a strong interfacial bonding between the particles. The composite exhibits desirable properties in terms of density (2.06 g/cm^3), hardness (124 BHN), impact energy (4.61 J), compressive strength (143.67 MN/m^2), shear strength (5.78 MN/m^2), thermal conductivity (0.39 W/mK), and wear rate (1.91×10^{-6} g/m). These values compare well with the properties exhibited by conventional/commercial brake pads indicating a potential for effective performance in service.

1. Introduction

In the past few years, the use of ceramic materials has significantly increased in various applications due to the superlative characteristics they exhibit compared with metals and polymers. The advantageous characteristics of ceramic materials include low density, high abrasive toughness, hardness, and rigidity. Nevertheless, monolithic ceramics main drawback is their low fracture toughness which leads to brittle fracture. Hence, many studies have been conducted with the aim of addressing this shortcoming (Oungkulsolmongkol et al., 2010; Aigbodion et al., 2010).

New challenges of modern high technology require the development of technical materials with combined properties or functions (Tarabay et al., 2013). Hence, particulate ceramic matrix composites have been developed to achieve damage tolerant fracture behaviour while maintaining other advantages of monolithic ceramics. It is established that particulate ceramic matrix composites (PCMC$_S$) are among those promising materials for high performance applications under severe environment such as high temperature. These materials offer the possibility of exhibiting high corrosion and wear resistance, mechanical strength, and thermal stability. PCMC$_S$ are nowadays the candidates for functionally graded materials developed for their multiple functions at reduced cost (Tarabay et al., 2013). They are used as functional components in brake assembly, furnace materials, energy conversion systems, gas turbines, heat engines, etc.

In an attempt to effect significant improvement in the functional characteristics of currently available brake pads of aircrafts and automobiles, different materials have been used and this has resulted in the development of different types of brake pads (Nagesh et al., 2014; Aderiye, 2014). This paper focuses on the synthesis and characterisation of a promising iron millscale particles reinforced ceramic matrix composite by powder metallurgy technique for automobiles and aircraft brake pad application.

2. Methodology

2.1. Materials and equipment

The reinforcement material used in this study is iron millscale particles while the matrices are silica sand, magnesia, and

* Corresponding author.
E-mail address: durosteve02@yahoo.com (S.I. Durowaye).
Peer review under responsibility of King Saud University.

Production and hosting by Elsevier

http://dx.doi.org/10.1016/j.jksues.2017.03.003

bentonite. Iron millscale particles were sourced from a steel manufacturer located in Ikeja, Lagos, Nigeria. Silica sand was obtained from the beach of the Lagos Atlantic Ocean. Magnesia and bentonite powders were obtained from a local vendor within the chemicals supplier trade group registered in Nigeria but were manufactured in China and Wyoming, USA respectively. Pictures of these materials are presented in Figs. 1 and 2.

Some of the major equipment and tools employed in the study include sieves, electric weighing balance, mixer, hydraulic press, oven, muffle furnace, compressive testing machine, hardness tester, Avery impact tester, thermal conductivity testing apparatus, wear tester, X-ray fluorescence, spectrometer, scanning electron microscope (SEM) with energy dispersive X-ray spectroscopy (EDS).

2.2. Ceramic composites production

2.2.1. Materials milling and blending

Iron millscale particles were milled using a steel ball mill (model A50 43, Mashine, France) and sieved to particles size distribution of 106–250 μm using standardised sieves (BSS). The matrix containing 212 μm silica sand, 53 μm magnesia, and 15 μm bentonite was separately mixed with the iron millscale particles and clean water amounting to 12 wt% of the total mixture was added. By manual mixing, a uniform distribution of reinforcement particles in the matrix blend was achieved and 80 g of wet blended materials formulation were fed into metallic moulds (Table 1).

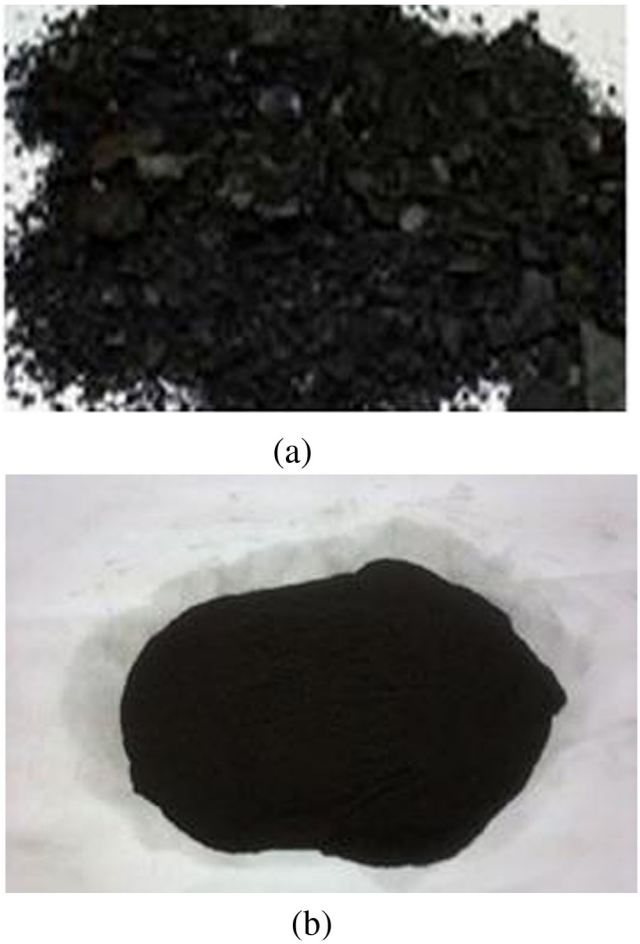

Fig. 1. Pictures of (a) as-received, (b) milled and sieved 106 μm iron millscale particles.

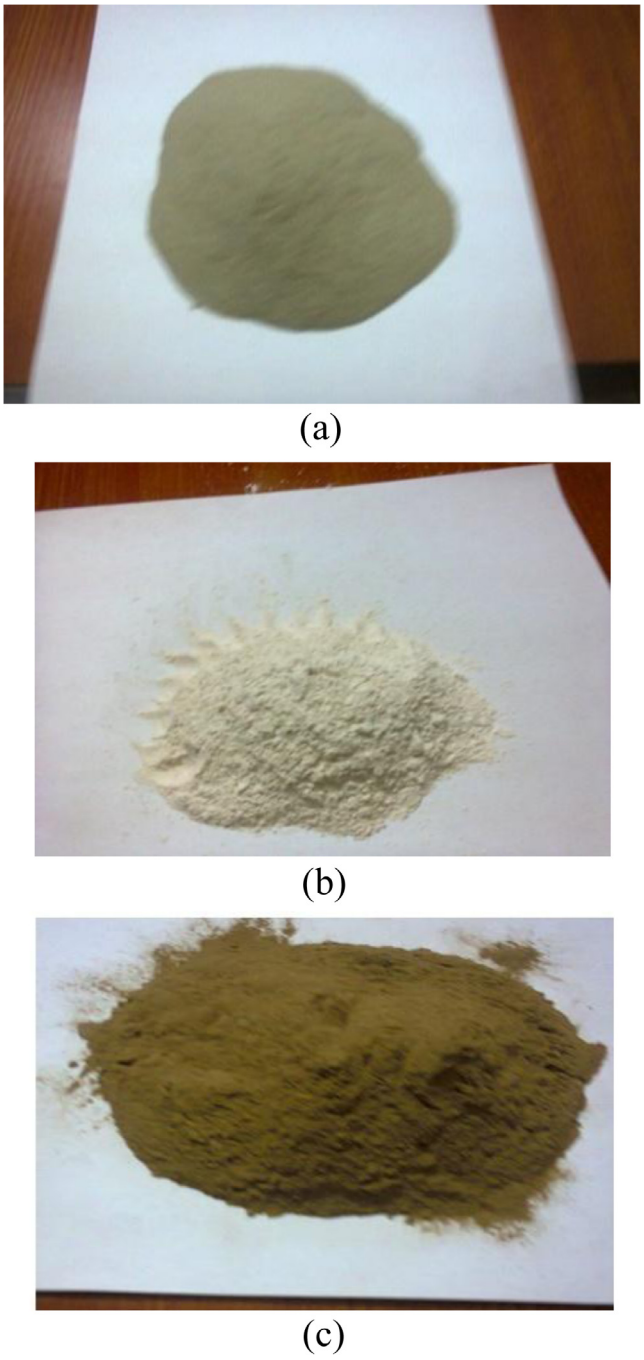

Fig. 2. Pictures of (a) milled and sieved 212 μm silica sand particles (b) as-received 53 μm magnesia powder, and (c) as-received 15 μm bentonite clay powder.

2.2.2. Compaction

The Green samples were obtained by uniaxial cold pressing (330 KN/m^2) using a hydraulic press (Capacity 100T, Type P100 EH, Model No. 38280, Weber Hydraulik, Germany) to enhance surface smoothness of the samples. Little quantity of lubricant was rubbed on the inner part of the moulds as a releasing agent to ease discharge of samples from the moulds after compaction.

2.2.3. Drying and sintering

The samples were dried in open air for 3 days, followed by drying under a controlled humidity using an oven dryer at 110 °C for 24 h to expel any moisture left in the composite and to avoid cracking during sintering. In order to facilitate the bonding of powder

Table 1
Materials formulation.

Iron millscale (wt%)	Silica (wt%)	Bentonite (wt%)	Magnesia (wt%)	Total (wt%)
0	30	30	40	100
3	29.1	29.1	38.8	100
6	28.2	28.2	37.6	100
9	27.3	27.3	36.4	100
12	26.4	26.4	35.2	100
15	25.5	25.5	34	100
18	24.6	24.6	32.8	100

Fig. 3. Picture of the produced ceramic composite.

particles, the compacted samples were gradually heated to temperatures below the melting point of the constituent materials but high enough to develop significant solid state diffusion. Sintering was carried out in a muffle furnace pre-set at heating rate of 10 °C/min in the following sequence: (i) heating to 600 °C, (ii) heating to 800 °C, (iii) heating to 1000 °C, and (iv) finally heating to 1200 °C. Samples were soaked at each heating stage for 3 h. They were removed from the furnace and allowed to cool after which they were characterised. The picture of few of the ceramic composites produced is presented in Fig. 3.

2.3. Properties evaluation tests

Weights of the samples in air were measured with an analytical balance and their weights in water were measured with a suspension kit and measuring cylinder at room temperature. The densities of the sintered samples were determined by Archimedes' principle based on buoyancy of water.

Scanning electron microscope (SEM), model ASPEX 3020 was used to determine the morphology of the samples at 15 kV.

Hardness test was conducted on the samples of dimension 25 mm × 25 mm × 10 mm in accordance with ASTM E10 standard using a Brinell hardness measuring machine. As the sample was mounted on the machine, a load of 5 kN was applied on it for about 10 s and the diameter of indentation left in the sample was measured with a low powered microscope. The Brinell harness number is calculated by dividing the load applied by the surface area of the indentation.

Impact energy test was carried out in accordance with ASTM D790 standard using an Izod impact tester. The samples were prepared to size of 55 mm × 10 mm × 10 mm with a 2 mm deep V-notch at the centre of the specimens. Each sample was clamped vertically with the notch facing the striker. The striking pendulum was allowed to swing downwards from a height of 1.3 m at a velocity of 5 ms^{-1} impacting the sample. The energy absorbed to fracture each specimen was read off from the instrument's dynamometer.

Compressive strength test was carried out on the samples dimensioned to 12.7 mm × 12.7 mm × 25.4 mm in accordance with ASTM D695 standard. Each of the samples was subjected to uniaxial compressive loading until the sample breaks and the strength is recorded using universal testing machine (UTM), Instron model 3369.

Shear Strength test was also carried out on the samples dimensioned to 25 mm × 25 mm × 10 mm in accordance with ASTM D7078 standard. Each sample was subjected to shear stress by v-notched rail shear using Universal Testing Machine, Instron Model 3369. The sample's face was clamped on both sides giving it a strong rigid hold as force is applied on the sample. The v-notches on the samples created localised and approximated uniform shear stress zone between the notches. A ± 45° two-element strain gauge was used to directly verify the shear strains applied.

The boiling method was used in determining the thermal conductivity of the samples. The thermal conductivity of the test samples was evaluated using the expression in Eq. (1) after measuring the relevant parameters.

$$\lambda = \frac{2.303 mc\delta \log \frac{T_s - T_1}{T_s - T_2}}{At} \quad (1)$$

where: λ is the thermal conductivity of the sample in (W/mK), 2.303 is a constant, Ts is temperature of steam (°C), T_1 is initial temperature of water in conical flask (°C), T_2 is final temperature of water in conical flask (°C), t is time (s), A is sample area (m^2), m is the mass of water in conical flask (kg), c is specific heat capacity of water in conical flask (J/kg °C), δ is thickness of sample (m).

A pin-on-disc test apparatus was used to investigate the dry sliding wear characteristics of the samples according to ASTM G99-95 standards. Wear tests were conducted with loads ranging from 8 to 24 N, disc speed of 250 rpm, and constant sliding distance of 1257 m.

3. Results and discussions

The major and minor constituents of the materials are shown in Table 2.

The SEM micrographs in Figs. 4a–7a show that the samples are made up of different additives which confirm that they are heterogeneous with differences in the geometry of the particles which are globular and needle-like. The EDS spectrographs show a good combination of the elemental distribution which also reflects on the heterogeneous nature of the composites. Different sizes of particles or elements also contributed to the heterogeneous distribution. The EDS spectrographs of most of the samples show the presence of O, Si, Al, Mg, Fe, and Ca but the unreinforced (control) does not contain Fe (Fig. 4b). There are also indistinguishable peaks in the spectrographs indicating the presence of other elements in very small amount.

The white spots in the micrographs are particles of the magnesia while the dark spots are FeO particles from the millscale. The ash coloured needle-like region is mullite ($3Al_2O_3{\cdot}2SiO_2$) while the gray mixed with whitish spots are the spinel as shown in Figs. 4a–7a. From the micrographs of the reinforced samples, FeO particles are seen to be well distributed in the matrix without any form of segregation. The interfacial bonding between the reinforcement and the matrix is enhanced by the relatively close-spacing of the FeO particles. This also suggests a good vitrification of the reinforced composites during sintering.

Table 2
Chemical composition of reinforcement and matrix.

Compounds	Amount (wt%)			
	Iron Millscale	Silica	Magnesia	Bentonite
FeO	68.81	0.02	–	–
Fe_2O_3	24.74	0.15	–	3.86
Fe_3O_4	6.18	–	–	–
SiO_2	0.01	98.99	0.01	62.99
MgO	0.02	0.02	98.84	2.67
CaO	0.22	0.02	0.03	1.32
MnO	0.02	0.01	–	–
Al_2O_3	–	0.18	–	23.25
Na_2O	–	0.01	–	2.46
K_2O	–	0.01	–	0.52
TiO_2	–	–	–	0.14
L.O.I	0.001	0.491	0.012	2.80
M.O.I	–	0.001	0.001	–

L.O.I = Loss on Ignition.
M.O.I = Moisture.

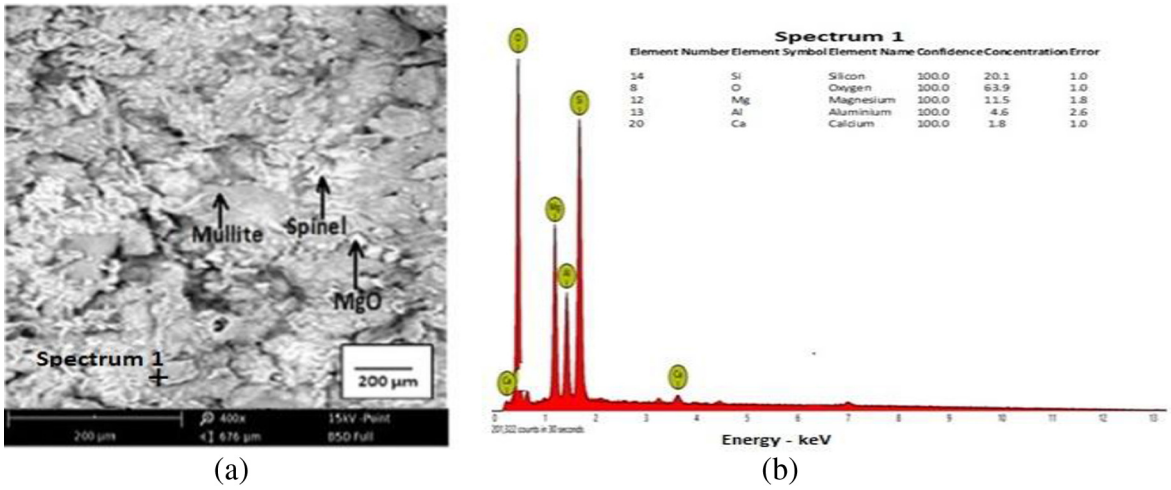

Fig. 4. (a) SEM (b) EDS of the unreinforced ceramic matrix composite (control).

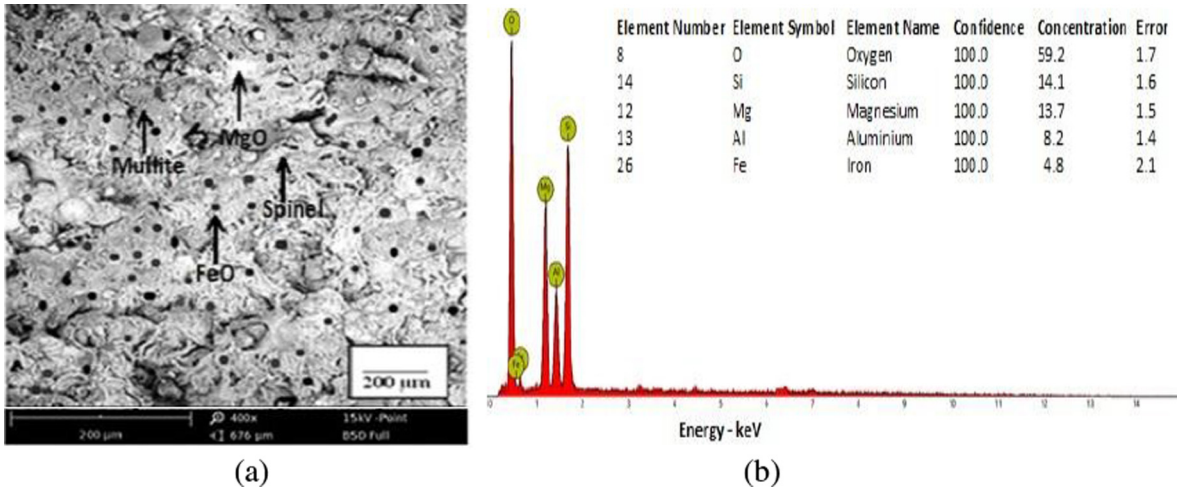

Fig. 5. (a) SEM (b) EDS of the 12 wt% 106 μm millscale reinforced ceramic composite.

There is a progressive increase in the density of the sample with increasing weight fraction of FeO particles addition as shown in Fig. 8. This behaviour is enhanced by the effective fusion of FeO particles during sintering with the ceramic matrix to form a coherent phase. This observation corroborates the maxim that iron based friction materials retain some particular properties among which is high density level (Asif et al., 2011).

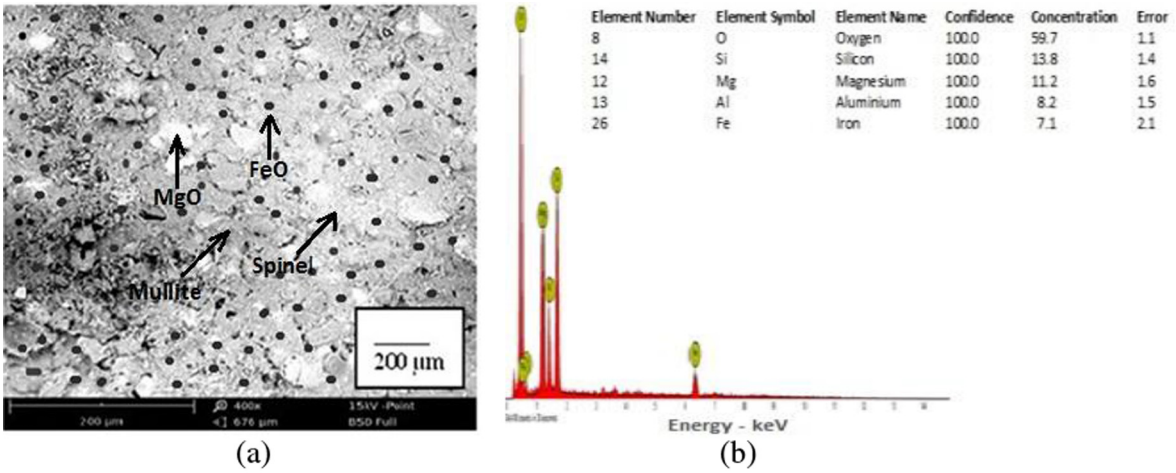

Element Number	Element Symbol	Element Name	Confidence	Concentration	Error
8	O	Oxygen	100.0	59.7	1.1
14	Si	Silicon	100.0	13.8	1.4
12	Mg	Magnesium	100.0	11.2	1.6
13	Al	Aluminium	100.0	8.2	1.5
26	Fe	Iron	100.0	7.1	2.1

Fig. 6. (a) SEM (b) EDS of the 15 wt% 180 µm millscale reinforced ceramic composite.

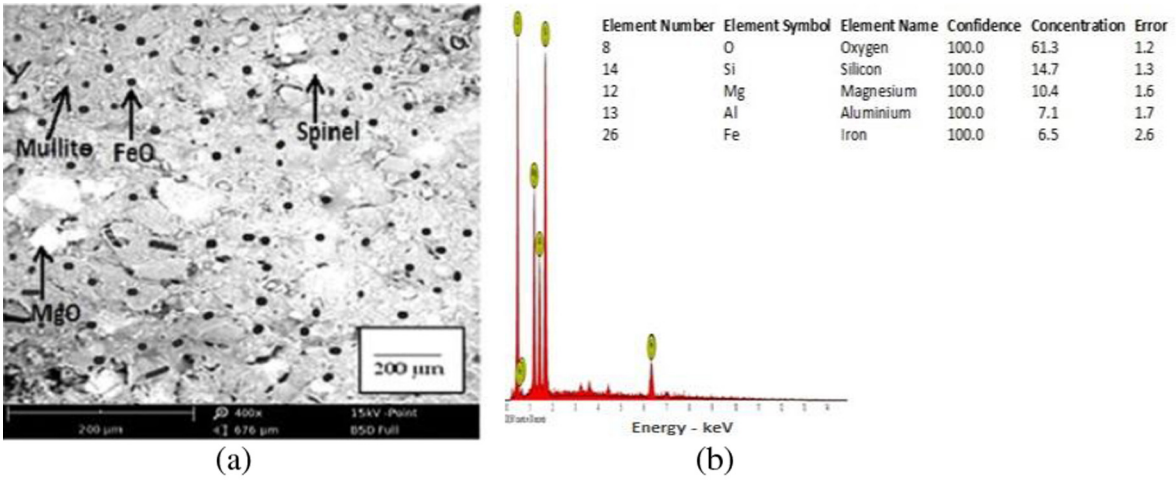

Element Number	Element Symbol	Element Name	Confidence	Concentration	Error
8	O	Oxygen	100.0	61.3	1.2
14	Si	Silicon	100.0	14.7	1.3
12	Mg	Magnesium	100.0	10.4	1.6
13	Al	Aluminium	100.0	7.1	1.7
26	Fe	Iron	100.0	6.5	2.6

Fig. 7. (a) SEM (b) EDS of the 15 wt% 212 µm millscale reinforced ceramic composite.

The density increment is also seemed to be due to deposition of iron as a result of diffusion into the ceramic phase which agrees well with the result of iron infiltration in ceramics as reported during In-situ TiC-Fe-Al_2O_3-TiAl/Ti_3Al composite coating processing using centrifugal assisted combustion synthesis (Mahmoodian et al., 2014). The density's range of 1.91–2.09 g/cm^3 composite samples is within the Nigerian Industrial Standards (NIS) specification of 1.99–2.25 g/cm^3 for automobiles brake pad (Dagwa and Ibhadode, 2006).

As shown in Fig. 9, the pore level of the unreinforced sample is 1.42% while the 106 µm reinforced sample has the lowest porosity of 1.12% at 15 and 18 wt% respectively. The decrease in the values of porosity with increasing weight fraction of millscale particles is due to strong interfacial bonding between the ceramic particles during high temperature sintering. This is supported by the work of Yawas et al. (2016). Low porosity enhances the achievement of compact and dense composite materials with the tendency to improve the mechanical properties (Ruzaidi et al., 2012). As a result of the low porosity exhibited by the samples, they have

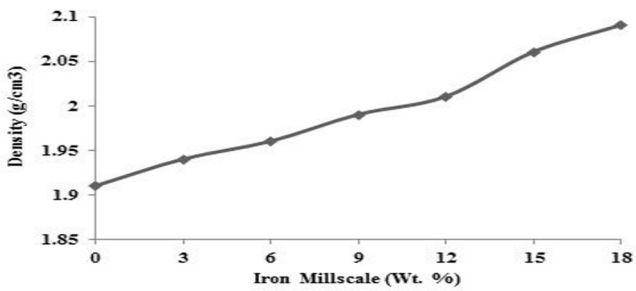

Fig. 8. Effect of varied iron millscale addition on the density of 106 µm millscale reinforced ceramic composites.

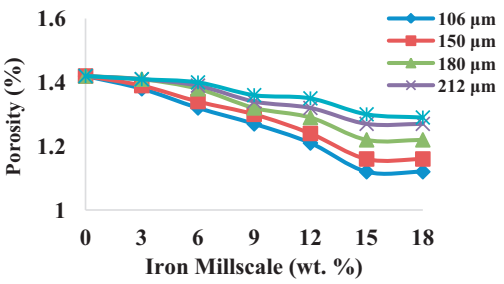

Fig. 9. Effect of varied iron millscale particles addition on porosity of the composites.

the tendency to exhibit high mechanical strengths, load bearing capacity, and resistance to corrosion (Callister and Balasubramaniam, 2011). The porosity of the developed composite compares well with the results of previous researchers using various materials to produce brake pads Fig. 10.

The hardness increases with decreasing particles size of iron millscale particles. However, the 106 μm iron oxide granules reinforced sample exhibits the maximum hardness values of 124 BHN (415 MPa) at 15 wt% reinforcement due to the influence of its smaller particles size. This agrees very well with the earlier work of Yawas et al. (2016). Small size particles enhance densification which enhances the mechanical properties better than coarse particles of the same concentration (Randelovic et al., 2012).

Generally, high hardness value of the composites is also due to the presence of hard materials SiO_2, MgO, Al_2O_3 (Aku et al., 2012). 101 BHN (≈335 MPa) is the hardness value of automobiles commercial brake pad (Dagwa and Ibhadode, 2006). The maximum hardness value of 124 BHN (415 MPa) obtained from the result of this study is higher than that of automobiles commercial brake pad. This is a strong indication that the sample will exhibit higher wear resistance than the commercial brake pad.

The impact energy of the samples decreases as the weight fraction of the iron millscale particles increases. The unreinforced sample has maximum impact energy of 6.07 J as shown in Fig. 11. The addition of a hard and brittle ceramic iron millscale particles (3–15 wt%) to the ceramic matrix increases the brittleness of the samples thereby reducing their ability to absorb energy. A slight increase in the impact energy of the samples is observed when reinforcement level is beyond 15 wt%. This may be due to the effect of increasing FeO content that is rich in iron which increased the plasticity of the composites thereby giving the samples plasticity to absorb energy (Kaundal et al., 2012). The 106 μm iron millscale particles reinforced composite exhibits better toughness than the other composites. This must have been due to the effect of the small particles size.

As evident from Fig. 12, there is an increase in the compressive strength of all the samples with increasing weight percentage of iron millscale particles addition from 0 to 18 wt%. The 106 μm iron millscale particles reinforced sample exhibits the maximum compressive strength (149.17 MN/m^2) at 15 wt%. Its small particles size must have contributed to this which is in agreement with established maxim that fine particles are more effective in strengthening composites than coarse particles of the same weight fraction (Randelovic et al., 2012).

The uniform distribution or dispersion of the hard FeO particles within the ceramic matrix results in a strong interfacial bonding which enhances the compressive strength of the composites. between the filler and the ceramic matrix giving rise to compressive strength enhancement. This increased the ability of the sample to restrain gross deformation. The average compressive strength of automobiles commercial brake pad is 110 MPa (Idris et al., 2015) while the recommended range for brake materials is 70–125 MPa (Dagwa and Ibhadode, 2006). The maximum compressive strength value of 149.17 MPa obtained in this study is higher than the recommended range and is also higher than the commercial brake pad.

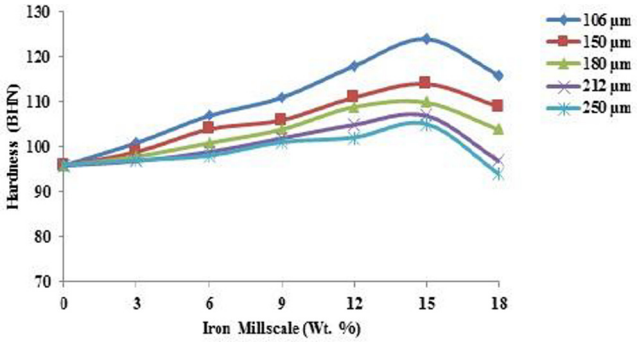

Fig. 10. Effect of varied iron millscale particles addition on hardness of the composites.

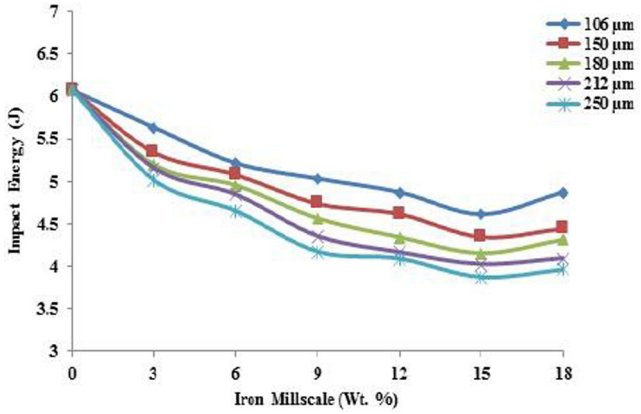

Fig. 11. Effect of varied iron millscale particles addition on impact energy of the composites.

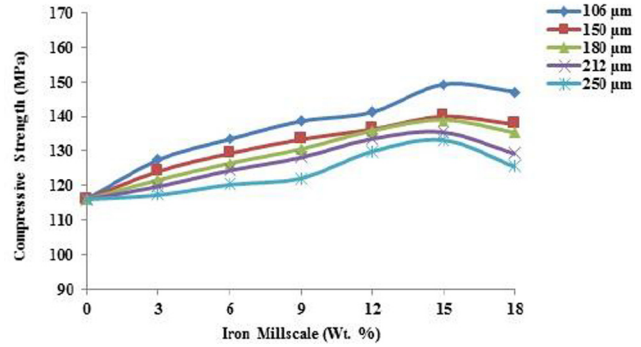

Fig. 12. Effect of varied iron millscale particles addition on compressive strength of the composites.

The shear strength is the amount of resistance the composite can offer against shear force that tends to cause sliding failure. It is evident from Fig. 13 that the samples demonstrate progressive increase in shear strength as iron millscale particles addition increases from 0 to 18 wt%. The 106 μm iron millscale particles reinforced sample exhibits the maximum shear strength value of 5.78 MN/m^2 at 15 wt% compared to 3.62 MN/m^2 of the unreinforced sample. The acceptable minimum shear strength of brake pad in the brake assembly is 4.9 MN/m^2 (Nagesh et al., 2014). Some of the samples exhibit higher shear strength than this value. The high shear strength exhibited is probably due to the effective synergy amongst the inputs through innovative processing. The uniform dispersion of the FeO particles in the ceramic matrix as shown in Figs. 5a–7a results in a strong interfacial bonding between the filler and the ceramic matrix also significantly enhance the samples shear strength.

The shear strength value of commercial brake pad is 5.46 MPa while the standard value is 2.10 MPa at room temperature for automobiles (Dagwa and Ibhadode, 2006). The maximum shear strength value of 5.78 MPa obtained in this study is higher than the commercial and standard brake pads values. These are indications

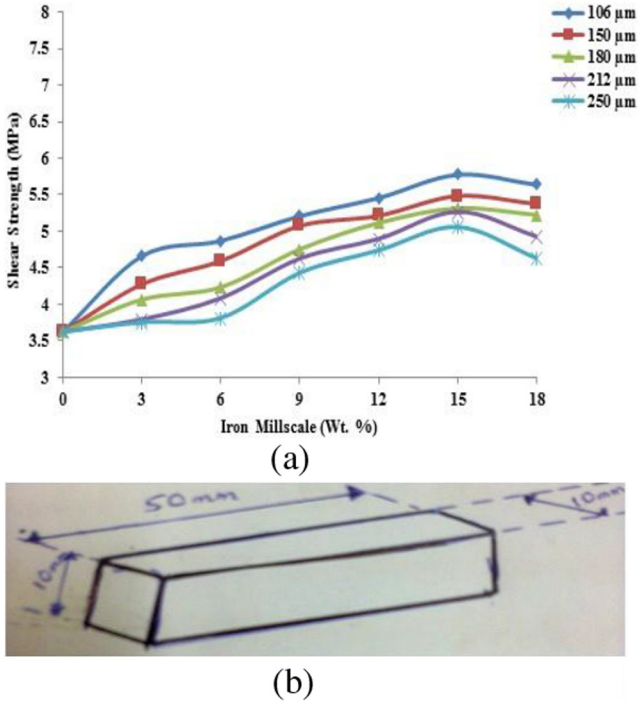

Fig. 13. (a) Effect of varied iron millscale particles addition on shear strength of the composites. (b) The schematic diagram of the shear test sample.

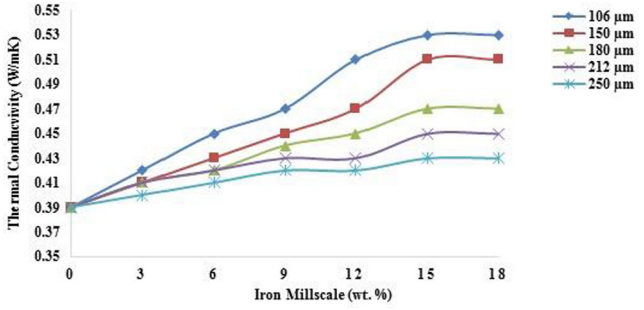

Fig. 14. Effect of varied iron millscale particles addition on thermal conductivity of the composites.

that the developed composite will perform well in service. The schematic diagram of the shear test sample is shown in Fig. 13.

There is a progressive increase in the thermal conductivity of all the composites with increasing wt% iron millscale particles addition from 3 to 18 wt% as shown in Fig. 14. The 106 µm iron millscale particles reinforced composite at 18 wt% exhibits the highest thermal conductivity of 0.53 W/mK. Generally, the standard thermal conductivity of friction materials (brake pads) ranges from 0.47 to 0.804 W/mK (Dagwa and Ibhadode, 2006). The thermal conductivity values of the developed composites are within the range of the standard values. The increase observed in thermal conductivity between the various particle sizes can be attributed to the increase in the surface area of the composites having comparatively fine particles which enables more particles involvement in thermal conductivity phenomenon.

Increase in density and decrease in porosity due to vitrification of the composites at high sintering temperature enhance the rate of heat transfer from one particle to another. These submissions agree with Lozano (2005) findings that the thermal conductivity of most ceramic materials greatly depends on the raw materials

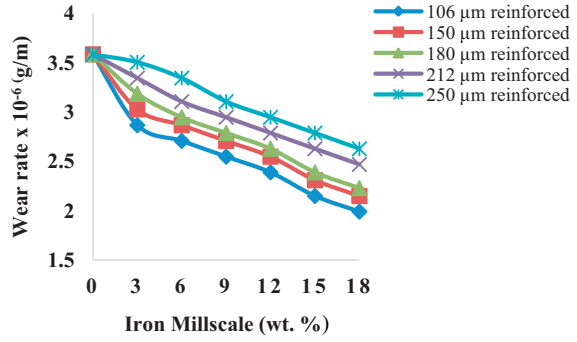

Fig. 15. Effect of varied iron millscale particles addition on wear rate of the composites.

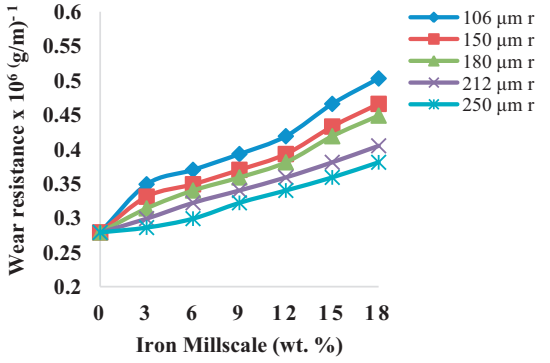

Fig. 16. Effect of varied iron millscale particles addition on wear resistance of the composites.

characteristics in terms of particle size distribution, processing route and other parameters such as temperature and pressure. According to Mahale et al. (2014), iron oxide (FeO) which is the closest to its equilibrium state and being the largest amount in millscale has the capacity for improved thermal conductivity. This predisposes iron millscale as a promising filler material in a heat generating environment thereby preventing possible addiabatic heating. This will prevent heat build-up that could cause warping of the brake pad.

The positive effect of the iron millscale particles size in reducing the wear rate and increasing the wear resistance can be seen in Figs. 15 and 16 respectively. The wear rate of the composites decreases with increasing millscale reinforcement. This also corresponds to increasing wear resistance as reinforcement increases. The range of the wear rate of the composites is from 1.99×10^{-6} to 3.58×10^{-6} g/m. The 106 µm millscale reinforced composite exhibits the lowest wear rate of 1.99×10^{-6} g/m at maximum load of 24 N. The wear rate of conventional brake pad is 3.8×10^{-6} g/m (Olabisi et al., 2016). The wear rate of all the composites is much lower than that of conventional brake pad. The decrease in wear rate of the composites is attributed to the diffusion of iron millscale particles and their deep penetration into the ceramic matrix. These result in a strong interfacial bonding between the ceramic matrix and millscale particles thereby forming a coherent phase with high wear resistance. The strong interfacial bonding significantly reduces the possibility of particles pull out. This agrees very well with the works of Idris et al. (2015) and Ikpambese et al. (2016). Improvement in wear resistance is mainly due to the increase in interphase bond strength and due to decrease in the number of microstructural flaws which are stress concentrators needed for nucleation and propagation of cracks.

4. Conclusions

From the results of investigation and discussion thereof, the following conclusions can be made:

1. A new iron millscale particles reinforced ceramic matrix composites suitable for application as automobiles and aircrafts brake pads have been successfully synthesised and characterised.
2. The 106 μm iron millscale particles reinforced composite at 15–18 wt% exhibits the highest thermal conductivity (0.53 W/mK), lowest wear rate (1.99×10^{-6} g/m), and highest mechanical properties in terms of density (2.06 g/cm^3), impact energy (4.61 J), compressive strength (149.17 MN/m^2), and shear strength (5.78 MN/m^2).
3. The low density confers light weight which will result to low fuel consumption by aircrafts and automobiles.
4. The desirable properties exhibited by the composites indicate a potential for effective performance in service as automobile/aircraft brake pads.

References

Aderiye, J., 2014. Kaolin mineral material for automobile ceramic brake pad manufacturing industry. Int. J. Technol. Enhance. Emerg. Eng. Res. 2 (3), 84–88.

Aigbodion, V.S., Agunsoye, J.O., Kalu, V., Asuke, F., Ola, S., 2010. Microstructure and mechanical properties of ceramic composites. J. Miner. Mater. Charact. Eng. 9 (6), 527–538.

Aku, S.Y., Yawas, D.S., Madakson, P.B., Amaren, S.G., 2012. Characterisation of periwinkle shell as asbestos-free brake pad materials. Pacific J. Sci. Technol. 13 (2), 57–63.

Asif, M., Chandra, K., Misra, P.S., 2011. Development of iron based brake friction materials by hot preform forging technique used for medium to heavy duty applications. J. Miner. Mater. Charact. Eng. 10 (3), 231–244.

Callister, W.D., Balasubramaniam, R., 2011. Materials Science and Engineering, 2011, seventh ed., Wiley India Pvt. Ltd., 4435-36/7, New Delhi-110002, India, ISBN 978-81-265-2143-2.

Dagwa, I.M., Ibhadode, A.O., 2006. Physical and mechanical properties of asbestos free experimental brake pad. Jormar 3 (2), 94–103.

Idris, U.D., Aigbodion, V.S., Abubakar, I.J., Nwoye, C.I., 2015. Eco-friendly asbestos free brake-pad: using banana peels. J. King Saud Univ. Eng. Sci. 27, 185–192.

Ikpambese, K.K., Gundu, D.T., Tuleun, L.T., 2016. Evaluation of palm kernel fibers (PKFs) for production of asbestos-free automotive brake pads. J. King Saud Univ. Eng. Sci. 28, 110–118.

Kaundal, R., Patnaik, A., Satapathy, A., 2012. Solid particle erosion of short glass fiber reinforced polyester composite. Am. J. Mater. Sci. 2 (2), 22–27. 5923/j.materials.20120202.05.

Lozano, F.M., 2005. Thermal conductivity and specific heat measurements for power electronics packaging materials. (Ph.D. thesis), Universitat Autonoma de Barcelona, Spain, pp. 1–204.

Mahale, P., Bohari, A., Raajha, M.P., 2014. Effect of thermal behaviour of friction materials on brake squeal. SAE Technical Papers. http://dx.doi.org/10.4271/2014-01-2514.

Mahmoodian, R., Hassan, M.A., Hamdi, M., Yahya, R., Rahbari, R.G., 2014. In-situ TiC-Fe-Al_2O_3-TiAl/Ti_3Al composite coating processing using centrifugal assisted combustion synthesis. Compos. B Eng. 59, 279–284.

Nagesh, S.N., Siddaraju, C., Prakash, S.V., Ramesh, M.R., 2014. Characterisation of brake pads by variation in composition of friction materials. Elsevier Proc. Mater. Sci. 5, 295–302.

Olabisi, A.I., Ademoh, N.A., Okechukwu, O.M., 2016. Development and assessment of composite brake pad using pulverized cocoa beans shells filler. Int. J. Mater. Sci. Appl. 5 (2), 66–78.

Oungkulsolmongkol, T., Salee-Art, P., Buggakupta, W., 2010. Hardness and fracture toughness of alumina-based particulate composites with zirconia and strontia additives. J. Metals Mater. Miner. 20 (2), 71–78.

Randelovic, M.S., Zarubica, A.R., Purenovic, M.M., 2012. New composite materials in the technology for drinking water purification from ionic and colloidal pollutants (accessed at doi: 10.5772/48390).

Ruzaidi, C.M., Kamarudin, H., Shamsul, J.B., Abdullah, M.M.A., 2012. Mechanical properties and wear behaviour of brake pads produced from palm slag. Adv. Mater. Res. 341–342, 26–30.

Tarabay, J., Peres, V., Serris, E., Valdivieso, F., Pijolat, M., 2013. Zirconia matrix composite dispersed with stainless steel particles: processing and oxidation behaviour. J. Eur. Ceram. Soc. 33, 1101–1110. Elsevier, SciVerse Science Direct.

Yawas, D.S., Aku, S.Y., Amaren, S.G., 2016. Morphology and properties of periwinkle shell asbestos-free brake pad. J. King Saud Univ. Eng. Sci. 28, 103–109.

Sekunowo is a seasoned metallurgical & materials engineer whose work-experience in the steel industry spanned sixteen years. In 2006, he joined the academic staff of the department of Metallurgical & Materials Engineering, University of Lagos, Nigeria where he has been actively involved in teaching and research. He is a senior lecturer. His research focus is mainly in the areas of developing innovative materials processing methods, characterisation and waste recycling (Value-addition engineering). He holds a Ph.D (Mechanical Metallurgy), a COREN (Council for the Regulation of Engineering practice in Nigeria) registered engineer and a corporate member of Nigerian Society of Engineers. He has over 40 research publications in international journals.

S.I. Durowaye is a metallurgical & materials engineer with 12 years of industrial experience. He is presently a lecturer in the Department of Metallurgical & Materials Engineering, University of Lagos, Nigeria. He is actively involved in teaching and research. He is a corporate member of the Nigerian Society of Engineers (MNSE). He has 20 research publications in international journals.

G.I. Lawal is a Professor of metallurgical & materials engineering in the Department of Metallurgical & Materials Engineering, University of Lagos, Nigeria. He has over 20 years of teaching and research experience. He is a member of the Nigerian Society of Engineers (MNSE) and other professional bodies. He has over 50 research publications in international journals.